Modeling thermal damage in skin from 2000-nm laser irradiation

Bo Chen
Sharon L. Thomsen
The University of Texas at Austin
Biomedical Engineering Laser Laboratory
Austin, Texas 78712
E-mail: chenbo@mail.utexas.edu

Robert J. Thomas
U.S. Air Force Research Laboratory
Optical Radiation Branch
Brooks City-Base, Texas 78235

Ashley J. Welch
The University of Texas at Austin
Biomedical Engineering Laser Laboratory
Austin, Texas 78712

Abstract. An optical-thermal-damage model of the skin under laser irradiation is developed by using finite-element modeling software (FEMLAB 3.1, Comsol, Incorporated, Burlington, Massachusetts). The general model simulates light propagation, heat generation, transient temperature response, and thermal damage produced by a radically symmetric laser beam of normal incidence. Predictions from the model are made of transient surface temperatures and the thermal damage on a pigskin surface generated by 2000-nm laser irradiation, and these predictions are compared to experimental measurements. The comparisons validate the model predictions, boundary conditions, and optical, thermal, and rate process parameters. The model enables the authors to verify the suitability of the American National Standards Institute (ANSI) maximum permissible exposure (MPE) standard for a wavelength of 2000 nm with exposure duration from 0.1 to 1 s and 3.5-mm beam diameter. Compared with the ANSI MPE standard, however, the MPE values predicted by the model are higher for exposure durations less than 0.1 s. The model indicates that it may be necessary to modify the ANSI MPE standard for cases in which the laser-beam diameter is larger than 3.5 mm when a "safety factor" of ten is used. A histopathological analysis of the skin damage is performed to determine the mechanisms of laser-induced damage in the skin. [DOI: 10.1117/1.2402114]

Keywords: damage threshold; finite element modeling; laser injury; laser safety; maximum permissible exposure; skin damage.

Paper 06026RR received Feb. 7, 2006; revised manuscript received Jul. 19, 2006; accepted for publication Jul. 19, 2006; published online Dec. 26, 2006.

1 Introduction

High-power laser systems operating at wavelengths of approximately 2000 nm, such as the Ho:YAG laser ($\lambda = 2.1\ \mu$m), are becoming increasingly important tools in the military, medicine, and industry. With the recent development of continuous-wave systems operating at 2000 nm, it may be necessary to refine the existing laser safety guideline limiting the exposure limits for these systems. Currently, the American National Standards Institute (ANSI) Z136.1-2000 guideline, *American National Standard for Safe Use of Lasers*,[1] gives the maximum permissible exposure (MPE) limits for far-IR wavelengths between 1.8 and 2.6 μm as a function of the duration of laser exposure. Because the MPE level for a wavelength of 2.0 μm was based on minimal experimental data, however, several damage threshold experiments have recently been conducted to refine the safe-exposure limits. In 2005, Zuclich et al. investigated the wavelength dependence of ocular thresholds in the near-IR and far-IR transition regions and noted that the exposure limits in some cases were above the measured damage thresholds in the band between 1.3 and 4.0 μm.[2]

In the present study, we conducted a series of experiments and tests on Yucatan mini-pigs to determine the effects of irradiated spot size and exposure duration on the threshold damage to skin from a laser beam with a wavelength of 2000 nm.[3] Instead of the more commonly used Yorkshire pigs,[3,4] Yucatan mini-pigs were used in this study because their skin has an anatomical similarity to human skin. During the experiments, 48-h damage thresholds were determined by probit analysis as functions of exposure time and spot sizes. The associated transient temperatures were measured with a thermal camera, and histological sections were taken for later analysis of the relationships among temperature, time, and damage. In this study, we validated an optical-thermal-damage model so that limited experimental data could be extrapolated to a wider range of laser conditions. The model, coupled with the 2.0-μm experimental data, provided a technique for evaluating laser safety standards.

The biological and physical changes in laser-irradiated skin depend on the temperature-time response of the tissue. The formation of a thermally induced lesion in the skin begins with the local absorption of laser light, which is converted into heat. The first mechanism by which the tissue is thermally affected can be attributed to alterations of physiological equilibria in response to the heat. As temperature increases, denaturation of proteins occurs, which leads to necrosis of

1083-3668/2006/11(6)/064028/15/$22.00

tissue and cells. Thermal coagulation, including collagen hyalinization, collagen and muscle birefringence changes, tissue whitening, and cell shrinkage, occurs at a higher temperature.[5]

Several published computer models have predicted heat generation, transient temperatures, and thermal damage in tissues, but few have compared predictions to measured temperatures.[6–18] In the 1970's, Mainster et al. used the finite-difference method to solve the heat conduction equation for cylindrical symmetrical, and thermal homogeneous media.[6,7] In 1971, Vassiliadis, Christian, and Dedrick developed a Green's function solution for symmetrical noncoherent sources.[8] Later, Welch combined a rate process model with the finite-difference model,[9] and Takata expanded the model to include multiple layers, blood perfusion, blister formation, and damage.[10,11] Cain and Welch tested the temperature predictions of the model for argon laser irradiation in a rabbit's eye and determined that the model was quite accurate in predicting measured retinal temperature and damage for laser-pulse durations exceeding 10 ms. In those models, the highly absorbing pigment epithelium was represented as a thin layer in a continuous medium with Beer's law absorption.[12] Torres and Motamedi modified the Takata skin model to predict the temperature response of an *in-vitro* aorta irradiated with an argon laser. In that study, the Beer's law heat source of the Takata model was replaced by a Monte Carlo model of photon propagation to account for light scattering. Even with that modification, however, Torres and Motamedi found that the computed steady state and relaxation temperatures were much higher than the measured results. A second set of experiments demonstrated the existence of temperature-dependent surface cooling associated with the evaporation of water at the surface of the skin.[18]

The study of the key factors associated with thermal injury and the evaluation of a wider range of exposure parameters are possible by modeling light propagation, heat generation, heat conduction, and temperature-dependent rate reactions and then validating the predictions with experimental data. In this work, we compare the results of our finite-element modeling of thermal damage to results obtained from our previous experiments.[3] Temperature distributions and damage are computed as a function of power, exposure duration, and spot size for the optical properties associated with 2000-nm irradiation of pigskin.

The extent of the damage to the surface was evaluated by visual inspection. In addition, for comparisons with the temperature and damage predicted by our thermal model, a qualitative histopathological study of the skin damage was performed to determine the mechanisms of laser-induced damage in the skin and to map the extent and severity of the lesions.

2 Materials and Methods

In our previous study, a series of experiments were conducted *in-vivo* on female Yucatan mini-pigs with dark skin to determine the damage thresholds for 2000-nm laser irradiation.[3] That limited study employed Gaussian-shaped beam diameters of approximately 5, 10, and 15 nm and exposure durations of 0.25, 0.5, 1.0, and 2.5 s as a function of laser power. The effects of each irradiation were evaluated shortly after exposure and 48 h later. The transient temperature distribution on the skin surface was measured with an IR-array thermal-detector camera for each combination of spot size and exposure duration.[3]

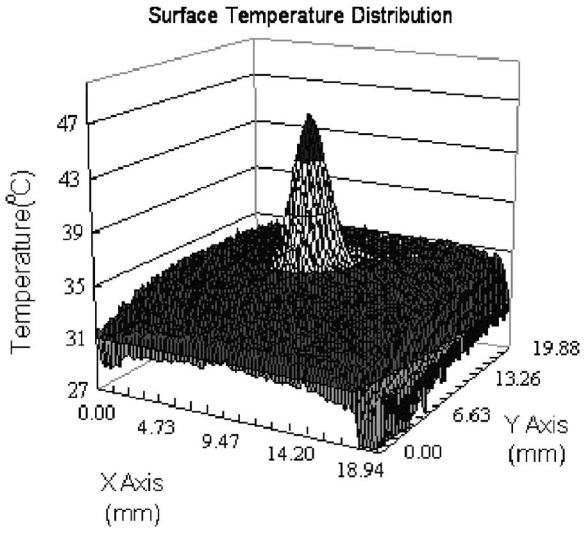

Fig. 1 Skin surface temperature distribution after 30-ms laser irradiation. Laser power is 3.23 W and beam radius is 2.44 mm.

2.1 *Preparation of Tissue Specimens*

The mini-pigs were euthanized 48 h after irradiation, at which time tissue specimens of each lesion were taken and fixed in 10% neutral buffered formalin, embedded with paraffin, sectioned, and stained with hematoxylin and eosin (HE). To determine the maximum histological diameter of the lesion in the skin, serial consecutive sections were cut through the sample blocks to locate the center of the thermal lesion at the microscopic level.

2.2 *Beam-Profile Measurement*

The laser beam spatial profile, which was critical for temperature modeling, was obtained by two methods: knife-edge measurement and spatial IR imaging of the skin by a 30-ms laser irradiation. The 1/e light penetration depth into the skin at 2000 nm was approximately 200 μm, and the associated characteristic thermal diffusion time for a large spot diameter was about 300 ms.[19] Compared to the characteristic diffusion time for skin, the heat conduction within the 30-ms pulse duration was insignificantly small. The temperature rise was directly proportional to the irradiance $[\mathrm{W/cm^2}]$ for the case of no heat transfer during the laser pulse. Therefore, the measured surface temperature distribution (Fig. 1) obtained from the thermal camera represented the spatial intensity profile of the nominally Gaussian-shaped laser beam. The spatial profile was elliptical rather than circular, with the major axis about 10% longer than the minor axis. The radial profiles along the two axes of the elliptic laser beam (see Fig. 2) were essentially Gaussian in shape with $1/e^2$ radii of 2.55 and 2.33 mm. The arithmetic average of the two radii was 2.44 mm, which was close to the knife-edge measurement value of 2.42 mm for this example. To simplify calculations, the model assumed that the spatial profile was a circular, symmetric, Gaussian beam with a $1/e^2$ radius of 2.44 mm.

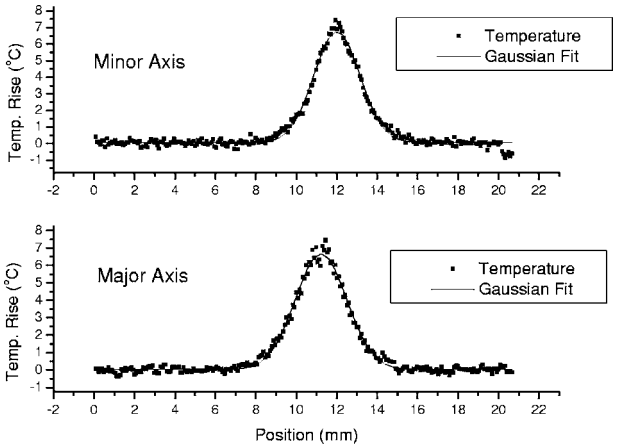

Fig. 2 Surface temperature distribution along major and minor axes after 30-ms laser irradiation.

The spatial profiles of two larger laser beams created with various telescopes were measured by using the spatial IR imaging as well as the knife-edge method. For the radii, the model used arithmetical averages of 5.04 and 6.92 mm derived from IR imaging. These two radii values were close to the knife-edge measurement values of 4.83 and 7.33 mm, respectively, values deviating by about 5% from the averaged radii. The differences in the values from these two methods were due to the elliptical, rather than circular, spatial profile assumed by the knife-edge measurement and the slight curvature of the mini-pig skin surface.

2.3 *Optical-Thermal-Damage Model*

An optical-thermal-damage model was developed by using FEMLAB finite-element modeling software (FEMLAB 3.1, Comsol Incorporated, Burlington, Massachusetts) to simulate the transient temperatures and thermal damage produced in skin by a radially symmetric laser beam at a normal angle of incidence. The skin was represented by two homogeneous regions (epidermis and dermis) with a nonlinear air-tissue boundary condition. Because the radially symmetric beam was perpendicular to the skin surface, the skin model was simplified to 2-D (radial r and axial z) and deployed using cylindrical coordinates. The FEMLAB model provided a time-dependent simulation that was capable of incorporating nonlinear boundary conditions and heterogeneous thermal and optical properties in tissue.

2.3.1 *Optical Propagation*

The formation of a thermally induced lesion in the skin was modeled as a temperature-time rate process associated with the thermal denaturation of proteins. The process began with the local absorption of the laser light by the skin and the conversion of the light into heat. The localized heat source $S[\mathrm{W/cm^3}]$ at position (r,z) and time t was a function of the local wavelength-dependent absorption coefficient $\mu_a(z)$ [1/cm], as follows:

$$S(r,z,t) = \mu_a(z)\phi(r,z,t), \tag{1}$$

where $\phi(r,z,t)[\mathrm{W/cm^2}]$ is the fluence rate at position (r,z) and time t. At 2000 nm, water was the primary chromophore in the skin. Because light scattering was insignificant at this wavelength, the model ignored scattering in the skin, and light propagation in the skin was described by Beer's law,

$$S(r,z,t) = \mu_a(1-r_s)E(r,t)\exp(-\mu_a z), \tag{2}$$

where $E(r,t)[\mathrm{W/cm^2}]$ was the irradiance and r_s was the specular reflectance on the skin surface. The specular reflectance of *in-vitro* mini-pig skin at the air/epidermis interface was measured as 4.75% by use of a spectrophotometer. Gaussian-distributed irradiance was used in the model to approximate the laser profile emitted from the 2000-nm laser system used in the experiments. The irradiance $E(r)$ was expressed as follows:

$$E(r) = \frac{2P}{\pi\omega^2}\exp\left(\frac{-2r^2}{\omega^2}\right), \tag{3}$$

where P is the radiant power [W] and ω is the $1/e^2$ radius of the laser beam.

2.3.2 *Heat Conduction*

It was assumed that there was no heat loss/gain because of blood flow and metabolism. The assumption was reasonable for our experimental conditions with exposure durations less than several seconds.[5,11,20] Therefore, the temperature response of the skin to laser irradiation was governed by the heat conduction equation:

$$\rho C\frac{\partial T}{\partial t} = \frac{k}{r}\frac{\partial T}{\partial r} + \frac{\partial}{\partial r}\left(k\frac{\partial T}{\partial r}\right) + \frac{\partial}{\partial z}\left(k\frac{\partial T}{\partial z}\right) + S, \tag{4}$$

where $T(r,z,t)$ [K] was the temperature in the skin, $\rho(z)[\mathrm{kg/m^3}]$ was the skin density, $C(z)$ [J/kg K] was the specific heat, and $k(z)$ [W/m K] was the thermal conductivity.

Water loss from evaporation was considered in the model boundary conditions. The evaporation occurred when water molecules near the surface experienced collisions that increased their energy above that needed to overcome the surface binding energy. The energy associated with the phase change was the latent heat of water evaporation. The energy required to sustain the evaporation came from the internal energy of the water, which experienced a reduction in temperature (the cooling effect).[21] Water evaporation was diffusion limited and highly dependent on the relative humidity of the air and temperature-dependent mass diffusion coefficients.[21] This approach for estimating the rate of free-water surface vaporization loss was based on the heat and mass transfer boundary layer analogy for evaporative cooling:[18,21,22]

$$Q_{\mathrm{vap}} = h_{fg}h_m(T_s)[\rho_{v,\mathrm{sat}}(T_s) - \rho_{v,\infty}], \tag{5}$$

where $Q_{\mathrm{vap}}(r,z=0)$ is the vaporization loss term $[\mathrm{W/m^2}]$, $\rho_{v,\mathrm{sat}}(T_s)$ is the mass density of saturated water vapor $[\mathrm{kg/m^3}]$ at the temperature of the tissue surface T_s, $\rho_{v,\infty}$ is the density of water vapor in the air $[\mathrm{kg/m^3}]$ at room temperature, h_{fg} is the phase-change enthalpy [J/kg] at T_s, and h_m is

the convection mass transfer coefficient [m/s]. Based on analogous heat and mass transfer mechanisms, this coefficient was obtained by applying the Lewis number:[18,21]

$$h_m(T_s) = h_e/[\rho_a(T_s)c_a(T_s)\mathrm{Le}^{2/3}], \quad (6)$$

where h_e is the heat-convection coefficient [$\mathrm{W/m^2\,K}$], which in this case is free convection; $\rho_a(T_s)$ is the density of the air [$\mathrm{kg/m^3}$]; $c_a(T_s)$ is the specific heat of the air [J/kg K]; and Le is the Lewis number for the diffusion of water vapor into air. The value h_{fg} was approximated as a constant value 2.35×10^6 J/kg. The value $\rho_{v,\mathrm{sat}}(T_s)$, which is a function of temperature on the skin surface, was estimated during the simulation using a fourth-order polynomial nonlinear fit of the published water-vapor thermal properties.[21]

$$\rho_{v,\mathrm{sat}}(T_s) = 4 \times 10^{-9} \times T_s^4 - 6 \times 10^{-8} \times T_s^3 + 1.96 \times 10^{-5} \times T_s^2 + 1.534 \times 10^{-4} \times T_s + 6.1098 \times 10^{-3}\ \mathrm{kg/m^3}.$$

where T_s is the surface temperature in Celsius [°C].

Because radiative loss on the surface is insignificant compared to the heat losses by convection and evaporation, the surface boundary condition was described by free convection and water evaporation:

$$-k\frac{\partial T}{\partial z} = h_e(T - T_\infty) + Q_{\mathrm{vap}}. \quad (7)$$

The model prediction of temperature rise as a function of time in response to laser irradiation agreed well with the experimental results when the value for h_e was 15 $\mathrm{W/m^2\,K}$. This value was in good agreement with typical values of h_e for free convection in air, which ranges between 5 to 25 $\mathrm{W/m^2\,K}$.[21]

The thermal properties of the epidermis and dermis were derived from the following equations[11] and the assumption of 80% water content in the dermis and 30% in the epidermis:[11]

$$\rho = (1.3 - 0.3w) \times 10^3[\mathrm{kg/m^3}],$$

$$C = \left(1.55 + 2800\frac{w}{\rho}\right) \times 10^3[\mathrm{J/kg\,K}],$$

$$k = \left(0.06 + 570\frac{w}{\rho}\right)[\mathrm{W/m\,K}], \quad (8)$$

where w is the water content.[11]

2.3.3 *Rate Process*

The standard rate process model of tissue damage was introduced by Henriques and Moritz in the 1940's. The damage parameter Ω, which indicates the level of damage, was computed using the Arrhenius equation:[23]

$$\Omega(r,z) = A\int_0^\infty \exp\left[\frac{E_0}{-RT(r,z,t)}\right]dt, \quad (9)$$

where A is the molecular collision frequency factor, E_0 is denaturation activation energy, and R is the universal gas constant. Henriques and Moritz assigned $\Omega = 0.53$ corresponding to a threshold of first-degree burn (persistent but reversible erythema), $\Omega = 1$ to the threshold of second-degree burn (irreversible partial-thickness injury), and $\Omega = 10{,}000$ corresponded to a threshold of third-degree burn (irreversible full-thickness injury). The original values for A and E calculated by Henriques and Moritz[23,24] were used in the model as follows:

$$A = 3.1 \times 10^{98}, \quad E = 628000\ \mathrm{J/mole}. \quad (10)$$

Table 1 Summary of thermal and optical properties used in the model.

Thickness [mm]	Epidermis[4]	0.068
	Dermis	1.432
Water content w[11]	Epidermis	0.3
	Dermis	0.8
Density, ρ [$\mathrm{kg/m^3}$]	Epidermis	1210
	Dermis	1060
Thermal conductivity k [W/m K]	Epidermis	0.20
	Dermis	0.49
Specific heat C [J/kg K]	Epidermis	2244
	Dermis	3663
Absorption coefficient μ_a [1/cm]	Epidermis	21.76
	Dermis	58.02
Molecular collision frequency factor A[23,24]		3.1×10^{98}
Denaturation activation energy E_0 [J/mole][23,24]		628,000
Heat-convection coefficient he [$\mathrm{W/m^2\,K}$]		15
Density of water vapor in the air at room temperature $\rho_{v,\infty}$ [$\mathrm{kg/m^3}$][21]		0.00865
Room temperature T_∞ [°C]		20

2.4 *Optical Property Measurements*

A method that used a transient temperature measurement was developed for measuring the *in-vivo* optical properties of the skin. Under conditions of insignificant heat conduction (exposure time, $t_0 \ll$ characteristic thermal diffusion time τ), the slope of peak temperature response to very short pulses versus time provided a measure of the absorption coefficient μ_a:

$$\Delta T(r,t) = \frac{\phi(r,z=0^+,t)\mu_a t}{\rho C}, \quad (11)$$

where $\phi(r,z=0^+,t)$ is the fluence rate just below the surface and t is the exposure time. The value ϕ was approximately equal to the incident flux $(1-r_s)E(r,t)$, since light scattering was insignificant (r_s was the specular reflectance). Because

Table 2 The ED50 average radiant exposure and standard deviation at damage thresholds defined as instant redness within one minute or persistent redness after 48 h. * are the thresholds of instant redness by observation within 1 min of irradiation. ** are thresholds of apparent persistent redness of the skin visible at 48 h after irradiation. # means estimated without using probit fit. ☆ means it did not fit trend.

	Radius(mm)					
	2.44		5.04		6.92	
Duration(s)	Instant (J/cm^2)*	Persistent (J/cm^2)**	Instant (J/cm^2)	Persistent (J/cm^2)	Instant (J/cm^2)	Persistent (J/cm^2)
0.25	2.83±1.23	3.50±0.37 #	2.42±0.19	2.65±0.33	1.96±0.26	2.67±0.07
0.5	4.60±1.02 ☆	3.98±1.28	1.84±1.37	3.10±0.17	2.50±0.14	2.81±0.27
1.0	3.80±1.23	4.97±1.55 #	2.64±0.03	3.61±0.44 #	2.65±0.60	3.34±0.70
2.5	3.07±1.07	5.48±1.60	4.14±0.28	4.42±0.34 #	3.46±0.55	4.09±0.50

the irradiance used in this measurement was constant during the laser pulse and had a Gaussian shape, the irradiance at $r=0$ $[E(r=0,t)]$ was equal to $2P/\pi\omega^2$ [see Eq. (3)]. P was the input power and ω was $1/e^2$ radius. Therefore, the absorption coefficient was estimated according to the slope of the peak temperature response curve during the first 100 ms of irradiation.

The thermal and optical properties of the epidermis and dermis used in the optical-thermal-damage model are summarized in Table 1.

3 Results

3.1 *ED50 Thresholds for 1-Minute and 48-Hour Observations*

A probit analysis[25] was conducted to estimate the ED50 thresholds according to two different end points of the thermal lesions: 1. instant redness observed on the skin within 1 min after laser irradiation, and 2. persistent redness at the site 48 h after irradiation.

Most of the lesions appeared immediately, that is, within 1 min of the onset of laser irradiation, and remained on the skin after 48 h. At some irradiation levels, which are close to the instant redness thresholds radiant exposure, however, several instant red spots recorded immediately after irradiations were not observed at the 48-h postexposure reading. At persistent redness thresholds, the redness at most of the irradiated spots had appeared within 1 min after irradiation. However, at some specific radiant exposure levels near the estimated persistent redness threshold, the redness developed on the skin several minutes after the laser irradiation ceased and persisted past the 48-h postexposure reading.

The average radiant exposure for the ED50 thresholds at the 1-min and 48-h postexposure readings are compared in Table 2. The radii used in the radiant exposure calculation were derived from the thermal image instead of the knife-edge measurement; therefore, the average radiant exposures listed in Table 2 are slightly different from the values presented in our previous work.[3] The standard deviation (σ) was derived from the probit fit curve by the following definition:

$$\sigma = (\mathrm{ED}_{84} - \mathrm{ED}_{16})/2, \tag{12}$$

where ED_{84} represents the dose for an 84% probability of laser-induced damage, and similarly for ED_{16}. At some irradiation conditions, direct estimations were made without a probit analysis, because the data were quite consistent and there was insufficient scatter for the probit program. In other words, there was consistent damage or no damage above or below the specific exposure levels (H_{yes} and H_{no}, respectively). In those limited cases, the ED50 value was estimated as the middle point between the lowest value of damage (H_{yes}) and largest value of no damage (H_{no}). The standard deviation of the ED50 value equaled 32% of the border width (H_{yes}-H_{no}).[3]

3.2 *Microscopic Observations of the Skin*

Figure 3 shows representative gross images of the mini-pig skin surface 48 h after various irradiations and their corresponding microscopic HE stained biopsies. Figures 3(a)–3(f) correspond to mini-pig skins without irradiation, irradiation at the radiant exposure level near the instant redness threshold, and radiant exposure at the persistent redness threshold, respectively. At the instant redness threshold, no redness was observed after 48 h [Fig. 3(c)] although redness had appeared immediately after irradiation. Mild perivascular edema and focal hyperkeratosis was found at some suspicious sites [Fig. 3(d)]; however, it was doubtful whether the lesion was caused by laser irradiation or mechanical trauma (scratching).

Figure 3(e) shows a gross image of the persistent redness. The thermal lesion formed flat red papules concomitantly with the shrinking of the epidermis at the center of the irradiation sites. The microscopic image of the injury is illustrated in Fig. 3(f). There was coagulative necrosis of varying depths at the burn site, with a loss of epidermis over some of the more severe burns. The pattern of necrosis had roughly the shape of

a flattened cone. The necrotic epidermis cells had pyknotic or shrunken dense nuclei or occasionally fragmented nuclei. Regenerated epidermis cells formed underneath the dead epidermis cells at the lesion boundary. Vascular dilation and thrombosis in the dermal blood vessels were observed, and perivascular inflammation appeared in deeper blood vessels.

3.3 *Absorption Coefficient of the Epidermis and the Dermis*

A dark mini-pig skin spotted with white areas was used to measure the *in-vivo* absorption coefficient. The peak temperature responses during the first 100 ms of laser irradiation were recorded with an IR camera with an imaging rate of 800 frames per second. The 1/e light penetration depth at 2000 nm was reported to be approximately 200 μm, and the associated characteristic thermal diffusion time for a large spot diameter was about 300 ms.[19]

Measurements ($n=10$) were conducted at two different locations on the mini-pig flank and at five different power levels. The absorption coefficient of the epidermis (μ_{a_epi}) for dark skin was 21.76 ± 0.99 cm^{-1}, which was derived from the slope of the linear fit lines of the peak temperature response curve using Eq. (11) (linear correlation coefficient $R\approx0.99$) (Fig. 4).

Because water was the primary absorber at the 2000-nm wavelength, another way to estimate the absorption coefficient of the epidermis was based on the product of absorption coefficient of water and the water content in the epidermis.

$$\mu_a = \mu_{\mathrm{water}} \times w, \tag{13}$$

where μ_{water} is the absorption coefficient of water, which is 69.12 cm^{-1} at 2000-nm wavelength[26] and w is the water content in tissue. Values of 80% for the water content in the dermis and 30% in the epidermis were used in the model. With those estimations, the calculated absorption coefficient of the epidermis was 20.74 cm^{-1}, which was in good agreement with the measured μ_{a_epi} (21.76 ± 0.99 cm^{-1}).

Absorption coefficients were also measured at two white areas on the spotted mini-pig skin. Those areas had less melanin density than the dark skin used more commonly in damage experiments. The measured absorption coefficient of the white skin was 21.03 cm^{-1}, which was close to dark-skin absorption coefficient of 21.76 cm^{-1}. This similarity indicated that melanin granules played an insignificant role in absorbing the far-IR 2000-nm wavelength.

From those results, a good assumption is that the absorption coefficient for the 2000-nm wavelength was directly proportional to the water content in the tissue. Consequently, the absorption coefficient of the dermis was estimated to be 58.02 cm^{-1}, according to the water content ratio of the dermis and epidermis as well as the measured absorption coefficient of the epidermis (μ_{a_epi}).

3.4 *Temperature Measurements Versus the Model Predictions*

To validate the optical-thermal-damage model, model predictions of the temperature response at the skin surface were compared to the experimental results. The peak temperature was defined as the maximum temperature at the irradiation site on the skin. Because of the Gaussian shape of the laser beam, the peak temperature represented the temperature at the irradiation center.

In Figs. 5(a)–5(c), the predicted peak temperatures after laser irradiation at various laser power levels are compared with the experimental results measured by the thermal camera. The predicted values for all exposure-duration and spot-size conditions agreed well with the experimental measurements within a 10% error.

Figure 6 is a comparison of the experimental and predicted peak transient temperature curves for the laser radiant exposures close to the persistent redness thresholds for various exposure durations. The predicted peak temperature rise followed the measured heating (with the laser on) curve quite well. After the laser was turned off, the predicted and experimental temperatures were in good agreement for the first 1 to 2 s. After that period, the computed curves deviated from the experimental results. We believe this deviation was due to our overpredicted cooling rate at a temperature below 50 °C.

3.5 *Damage Predictions by the Model*

In the standard rate process model, threshold damage was associated with a second-degree burn (irreversible partial-thickness injury), and parameters were selected so that $\Omega=1$ at the boundary of damage and normal tissue. In our experiments, this definition corresponded to the threshold occurrence of a persistent redness lesion on the skin. Therefore, the model calculated Ω values and defined a contour line of $\Omega=1$ as the persistent redness lesion boundary. Within this boundary, Ω was greater than 1. Thus, there was a region of super threshold damage according to the damage integral. Experimentally determined threshold energy levels do not correspond to $\Omega=1$ at the center of the laser spot ($r=0$). In practice, a finite area and a boundary of damage are necessary for an observer to determine that damage has occurred. Therefore, threshold damage becomes a function of the method of observation and the observer's ability to see a thermally induced change in natural skin. The following results were based on that definition.

The model predicted thermal lesion boundaries that were bowl shaped. A comparison of the computed surface radii with experimental measurements is given in Table 3, and the computed depths are listed in Table 4. Because the ED50 damage threshold power levels usually did not correspond exactly to power levels used in the experiments, a corresponding experimental radius did not exist. The experimental damage radii were estimated using the measurements at the first lower and first higher experimental power levels near the thresholds. A sample of the measured radii of redness versus power levels is shown in Fig. 7. An example of a probit fit analysis for damage/no damage as a function of power is illustrated in Fig. 7 as well. The predicted temperatures at the thermal lesion boundaries after laser irradiation were compared for various spot sizes and exposure durations [Figs. 8(a) and 8(b)].

Another end point of the damage threshold, namely, the instant redness at the 1-min observation point, was analyzed using the optical-thermal-damage model. The maximum computed Ω values at both r and z equal to zero for the radiant

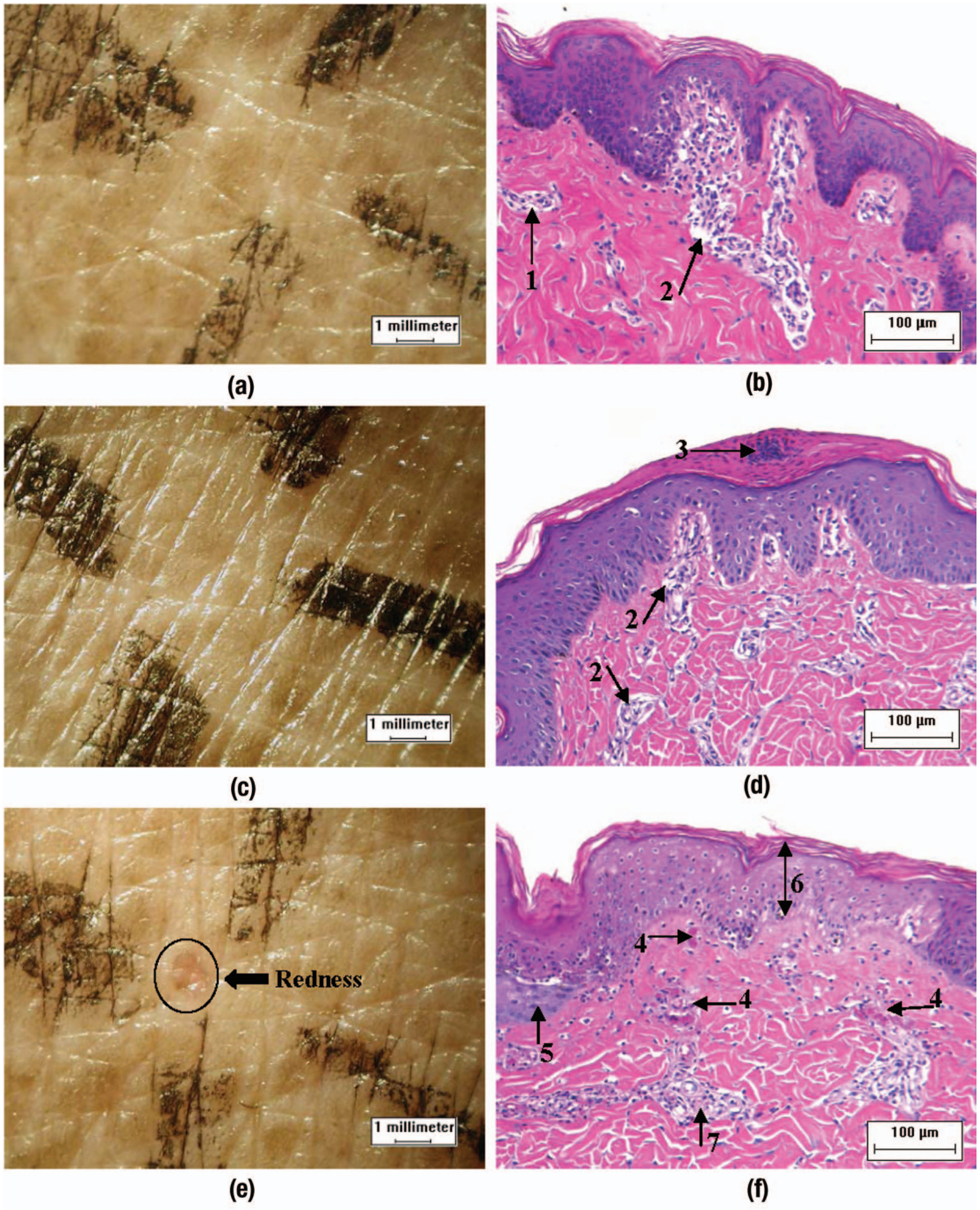

Fig. 3 The gross pictures of mini-pig skin surface 48 h after various irradiation and their corresponding microscopic biopsies (HE stain, original magnification 200×). (a) and (b): no irradiation. (c) and (d): irradiation at the radiant exposure level close to the instant redness threshold (exposure time 2.5 s, beam radius 2.44 mm, and laser power 0.29 W). (e) and (f): irradiation at persistent redness threshold (exposure time 2.5 s, beam radius 2.44 mm, and laser power 0.41 W). Note in (b): normal dermal blood vessels (arrow 1), edema and inflammation (arrow 2). Note in (d): edema and inflammation (arrow 2), focal hyperkeratosis (arrow 3). Note in (f): vascular dilation and thrombosis in dermal blood vessels (arrow 4), regenerated epidermal cells growing under necrotic epidermis (arrow 5), transmural necrosis of epidermis (arrow 6), and perivascular inflammation (arrow 7). In conclusion, all blood vessels show edema and inflammation; however, thrombosis, transmural epidermal necrosis, and dermal vascular dilation were not observed in (b) and (d).

exposure at the instant-redness thresholds are given in Table 5.

In the far-IR wavelength range of 1.800 to 2.600 μm, the ANSI Z136.1-2000 defined MPE as follows:

$$H_{\max} = 0.56t^{0.25}, \tag{14}$$

where $H_{\max}$ is the maximum radiant exposure and t is the exposure duration. The standard is specified for a limited spot

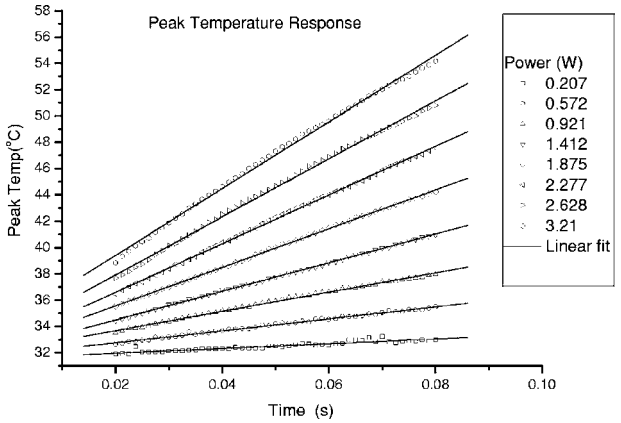

Fig. 4 Linear fits of peak temperature response curve during the period of no heat conduction.

diameter of 3.5 mm and exposure durations between 10^{-3} to 10 s.[1]

MPE values have usually been assumed to be a factor of 10 below the radiant exposures at damage thresholds. Inversely, the threshold radiant exposures for various exposure durations were estimated to be ten times the current ANSI MPE values. Using the optical-thermal-damage model, this study examined the damage for those radiant exposures. The radii and depths of damage boundaries ($\Omega=1$) that were simulated are listed in Table 6.

The optical-thermal-damage model was modified to predict CO_2 laser (10.6-μm wavelength) damage thresholds. The absorption coefficients of the epidermis and the dermis were estimated as 256.44 and 683.84 cm^{-1}, respectively, based on the product of the water absorption coefficient (854.8 cm^{-1} at 10.6 μm wavelength[26]) and water content in the epidermis and the dermis. Instead of using Gaussian beam irradiance, a 1.9-cm flat-top laser beam was employed in the model to simulate the laser profile used in the published pigskin laser threshold damage experiments.[27] Simulation determined the threshold radiant exposure, which produced $\Omega=1$ within 9 mm of the beam center. Figure 9 is a comparison of the simulated damage thresholds and the pigskin damage threshold data.[27] The predicted damage thresholds for 10.6-μm (CO_2 laser) and 2.0-μm laser irradiation as a function of exposure duration are compared in Fig. 10. The corresponding ANSI MPE limits for these wavelengths are drawn in Fig. 10 as well.

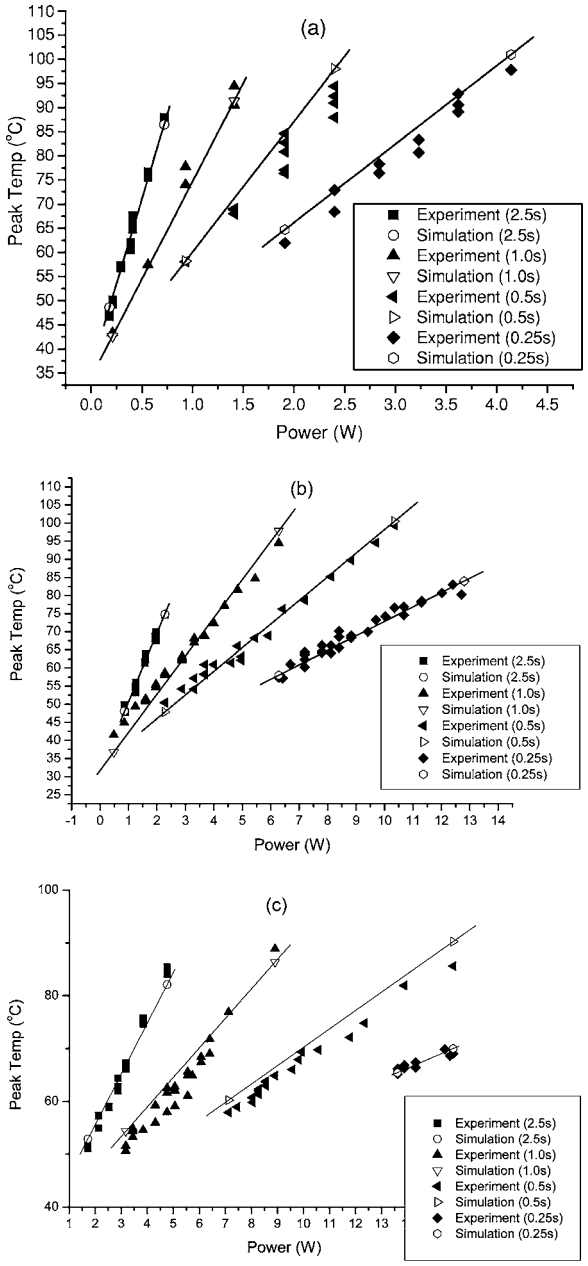

Fig. 5 The predicted and experimental peak temperatures after laser irradiation for various exposure durations and (a) 2.44-, (b) 5.04-, and (c) 6.92-mm spot radii.

4 Discussion

4.1 *Histological Analysis of Instant and Persistent Redness in Skin*

The average radiant exposures for the ED50 thresholds for instant and persistent redness at the sites of irradiation are compared in Table 2. Overall, the average radiant exposures for the instant redness thresholds were lower than for the persistent redness thresholds. Gross observations also found that at some of the sites irradiated with radiant exposures near the instant redness thresholds, redness developed on the skin immediately after the irradiation but gradually disappeared after several hours.

Histologically, the instant and persistent redness observed on the skin suggests different damage mechanisms are at work. The laser-induced temperature rise in the skin causes a dilation of the blood vessels and an increase in the number of open vessels in the dermis. The resulting increase in blood perfusion transfers more heat out of the high-temperature region to cool the skin to normal temperature.

Instant redness from hyperhemia is a reversible injury, and in this study the skin with instant redness reverted to its normal state after only a few hours without any persistent damage. The HE stained biopsies of the skin sites where redness appeared immediately after irradiation but not after 48 h did not present evidence of specific persistent injury [Figs. 3(c)

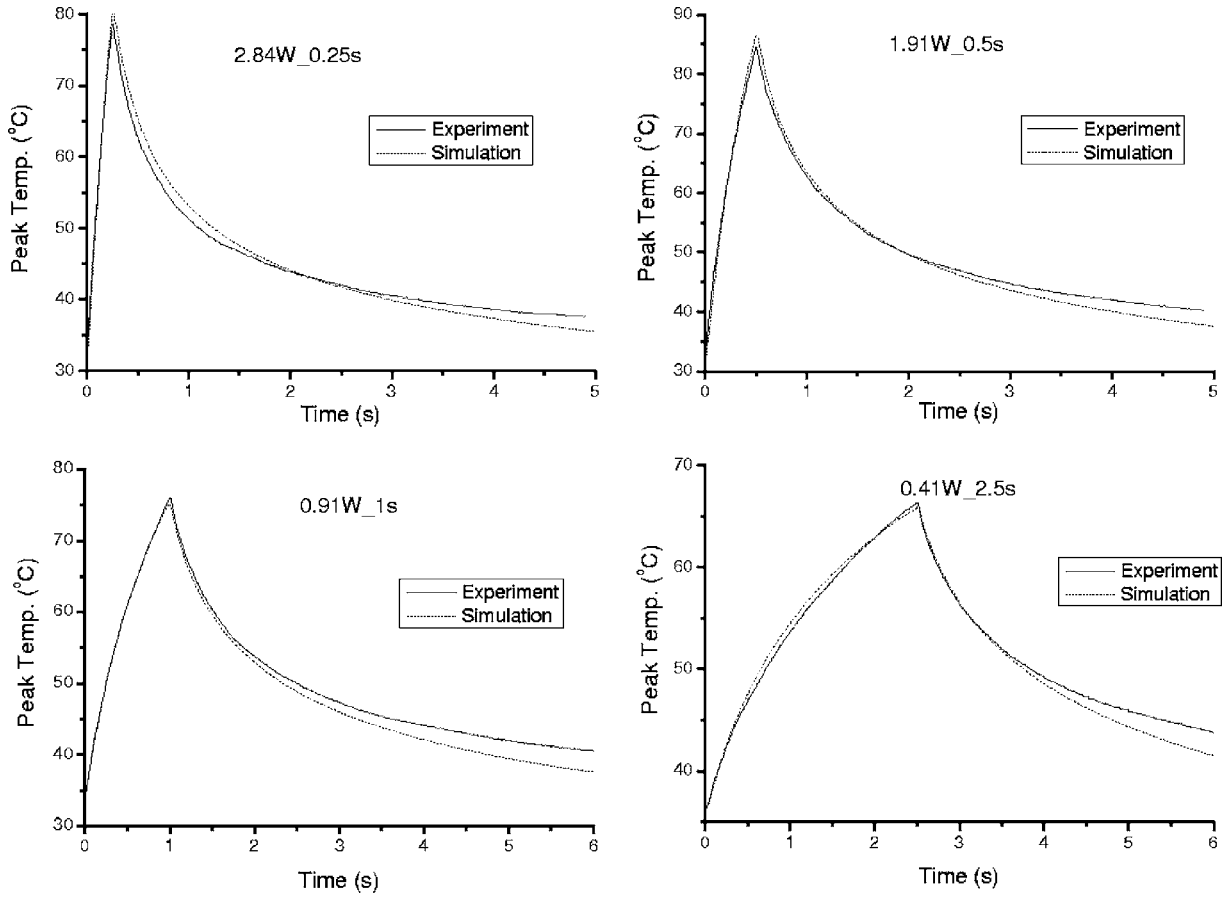

Fig. 6 The experimental and predicted peak temperature responses by laser irradiation of various durations. Beam radius is 2.44 mm.

and 3(d)]. At some higher input of radiant exposure, the temperature reached a critical point where irreversible redness damage was generated. In other words, a site where a persistent redness was observed 48 h after the irradiation represented a more serious thermal injury to the skin. At persistent redness thresholds, the 2000-nm wavelength laser irradiation produced death and necrosis of the epidermal cells and lethal thermal damage to superficial blood vessels. These results were the outcomes of a complex series of physiological vascular responses to heat, including the following: 1. hemostasis (blood flow stasis), 2. thrombosis, and 3. vascular dilation [see Figs. 3(e) and 3(f)]. In the dermis, some cellular elements were more sensitive to injury than others, and they were necrotic at a greater depth than the resistant tissues. Thus, there were no sharp edges to the burn lesions. The endothelia of the blood vessels and supporting tissues were more sensitive than other tissues. The collagen bundles below the epidermis were swollen but there was no change in birefringence image in-

Table 3 Radii of persistent redness on surface by experimental observations and model predictions using the threshold radiant exposure for persistent damage give in Table 2. * means the computed radii from threshold radiant exposure did not follow the expected trend.

	Radius(mm)					
	2.44		5.04		6.92	
Duration(s)	Simulation (mm)	Experiment (mm)	Simulation (mm)	Experiment (mm)	Simulation (mm)	Experiment (mm)
0.25	1.03	0.75 to 2.5	1.04	0.5 to 1.0	2.29	0.5 to 2.0
0.5	0.99	0.5 to 2.5	1.06	0.75 to 1.5	1.20	0.5 to 1.0
1.0	1.09*	0.75 to 1.0	0.77	0.5 to 1.5	1.51*	1.0 to 1.5
2.5	0.71*	0.5 to 0.75	0.58	0.5 to 1.25	0.58	0.5 to 2.0

Table 4 Predicted maximum depths of thermal lesions at threshold radiant exposure computed for $\Omega=1$.

	Radius(mm)		
Duration(s)	2.44	5.04	6.92
0.25	0.26 mm	0.16 mm	0.22 mm
0.5	0.28 mm	0.18 mm	0.17 mm
1.0	0.36 mm	0.18 mm	0.22 mm
2.5	0.32 mm	0.20 mm	0.14 mm

tensity. When heated, the complex type 1 collagen macromolecules and fibrils undergo several configuration changes, depending on the tissue temperature and time at temperature. Thermally associated swelling of the collagen fibers seen at the light microscopic level is associated with an expansion of the collagen fibril diameters due to radial dissociation of the collagen macromolecules detected in transmission electron micrographs. This swelling seen at lower temperatures, as shown in *in-vitro* experiments of rat skin heated at 50 °C for 1000 s, is not associated with birefringence image intensity loss. Total birefringence loss occurs at 60 to 65 °C under the same experimental conditions.[28]

4.2 *Predicted Thermal Damage*

Good agreement between the results from the optical-thermal-damage model and the experimental results indicated that the model had included the major parameters contributing to the thermal response of the skin to 2000-nm laser irradiation. The discrepancy between the predicted and measured temperatures a few seconds after the laser was turned off is hypothesized to be attributable to surface drying, which reduces the evaporative cooling effect (Fig. 6). The difference between measured

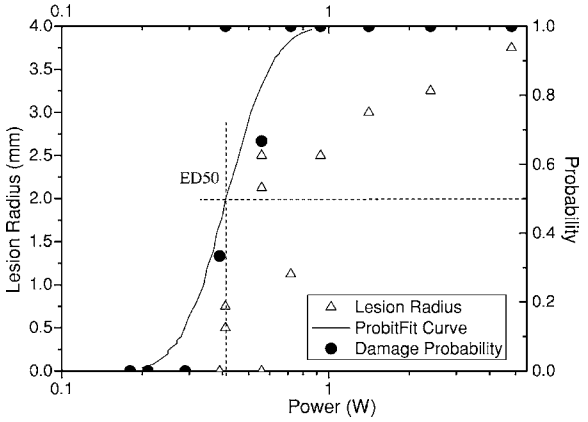

Fig. 7 Radii of redness lesions and the probabilities of thermal damage versus power levels. The triangles are the radii of the redness lesions that appeared on the skin after 48 h. The circles are the experimental data (the probabilities to find damage after irradiations) and the solid curve is the probit fit curve of the lesion/no-lesion observation as a function of laser power. Zero represents no damage and one represents damage. Some circles are not zero or one due to the variation of multiple measurements at the same power. Laser condition: exposure time 2.5 s and beam radius 2.44 mm.

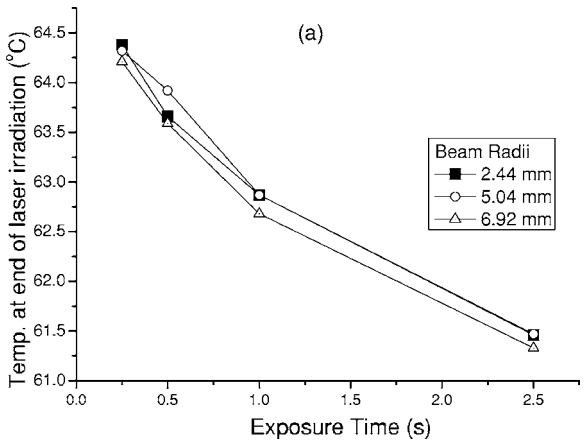

Fig. 8 (a) Predicted surface temperature at the end of the laser irradiation at the lesion/no-lesion boundary ($\Omega=1$). Lesion radii are given in Table 3. (b) Predicted temperature at the end of the laser irradiation at $r=0$, $z=$max predicted lesion depth at $\Omega=1$. Maximum lesion depths are given in Table 4.

and computed temperature appeared several seconds into the relaxation phase, typically, when temperatures were less than 50 °C, at which point the damage term $\exp[E_0/RT(t)]$ of Eq. (9) did not significantly impact the damage integral. In other words, for exposure duration of less than 2.5 s, the predicted temperature transient and the rate process algorithm were sufficient to predict thermal damage with negligible error. However, for longer exposure durations, the boundary condition must be adjusted to reflect the reduced heat loss as the skin surface dries.

The predicted radial temperature distribution was compared to the experimental temperature distributions along the major and minor axes of the experimental irradiance profile at the end of laser irradiation exposure durations of 0.25, 0.5, 1.0, and 2.5 s (Fig. 11). The circular beam profile simplification did not cause the simulated temperature distributions to significantly deviate from experimental temperature distributions. Near the center of the beam where temperatures are maximum, a couple of degrees difference between computed and measured temperatures would produce a significant error in the value of the damage integral Ω. However, at the boundary of threshold damage (typically 1-mm radius in our experiments), the difference between computed and measured tem-

Table 5 Predicted maximum Ω values at instant damage threshold radiant exposure (at $r=0$, $z=0$). ☆ means the experimental threshold radiant exposure did not fit the trend.

	Radius (mm)		
Duration(s)	2.44	5.04	6.92
0.25	32.65	1.15	0.280
0.5	1.27e5 ☆	8.4e−4	5.048
1.0	14.1	0.013	0.183
2.5	0.004	6.01	0.088

Table 6 Predicted radii and depths of thermal lesions ($\Omega=1$) with radiant exposures (ten times ANSI MPE values $H_{max}=0.56t^{0.25}$) and 3.5-mm laser spot diameter.

Duration(s)	10	1	0.1	0.01	0.001
Radius (mm)	$\Omega_{max}<1$	0.93	0.88	0.36	$\Omega_{max}<1$
Depth (mm)	$\Omega_{max}<1$	0.45	0.27	0.13	$\Omega_{max}<1$

peratures is smaller; moreover, at this lower temperature range, the contribution to the damage integral is more time dependent.

The predicted radii of surface lesions and their experimental counterparts were compared in Table 3. The radii of surface spots with persistent redness were measured by an experienced clinical pathologist 48 h after irradiation. Because of the uncertainty of the redness determination and the diversity of mini-pig skins, the measured radii near thresholds varied over a relatively large range. (A sample of measured radii of redness versus power levels is shown in Fig. 7). Typically, predictions were within the range of experimental results. The experimental data indicated that the lesion sizes at thresholds had approximately 1-mm radii but with a rather large range of values. Overall, the trend of the computed radii in Table 3 showed that damage radius (at $\Omega=1$) was directly proportional to spot size and inversely proportional to exposure duration. Exceptions to this trend are marked by * in Table 3. At those points, the threshold radiant exposures may have been overestimated; that is, the computed lesion radius using the experimental threshold radiant exposures did not conform to the expected trends. The probit analysis of the experimental data indicated that the relative errors (the ratio of standard deviation and mean value given in Table 2) of these three threshold radiant exposures were over 20%. For our largest spot size (radius=6.92 mm), the range of radii for experimental lesions was the largest. As spot size increased, the radial gradient of the temperature decreased. Thus, measurement uncertainty was amplified by the nonuniformity of the native tissue; that is, the tissue was not homogeneous. Owing to this nonhomogeneous nature of the skin, we did not have circularly symmetrical lesions. even though the Yucatan mini-pig skin best approximates the properties of human skin, the dark pigmentation of the skin hindered the gross visual determination of threshold damage, and therefore may have contributed to an uncertainty in the threshold value because of observational threshold differences, especially for large laser spots and short exposure durations.

The predicted depths of the lesions at thresholds are listed in Table 4. The predicted values indicated that damage from 2000-nm wavelength laser irradiation would be confined to a very thin layer with a thickness less than 360 μm. The HE stained skin biopsies (Fig. 3) revealed coagulative necrosis in the epidermis and blood vessel damage with thrombosis and stasis of blood in dilated blood vessels at the burn sites. The pattern of necrosis was roughly the shape of a flattened cone. Epidermis cells had pyknotic or shrunken dense nuclei or occasionally fragmented nuclei, which were morphological evidence of cell death and necrosis.

The predicted temperatures at the end of the laser irradiation at the predicted damage boundary (Table 3) were computed for the threshold radiant exposure of each spot size-exposure duration condition [Figs. 8(a) and 8(b)]. As expected, a smaller temperature rise was needed to generate thermal damage for longer exposure durations. Temperatures after irradiation at the damage boundary decreased concavely from 64.3 to 61.4 °C, whereas exposure duration increased from 0.25 to 2.5 s, respectively. Only a 3° change in temperature occurred for a change in irradiation time by a factor of

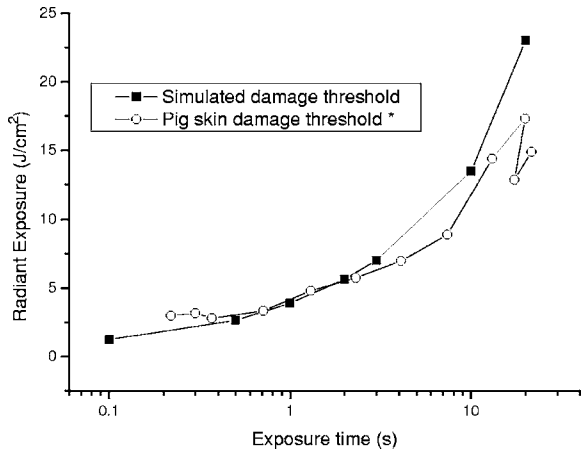

Fig. 9 The simulated damage threshold radiant exposures to CO_2 laser irradiation compared to published pigskin damage thresholds data as a function of exposure duration. * refers to Ref. 30.

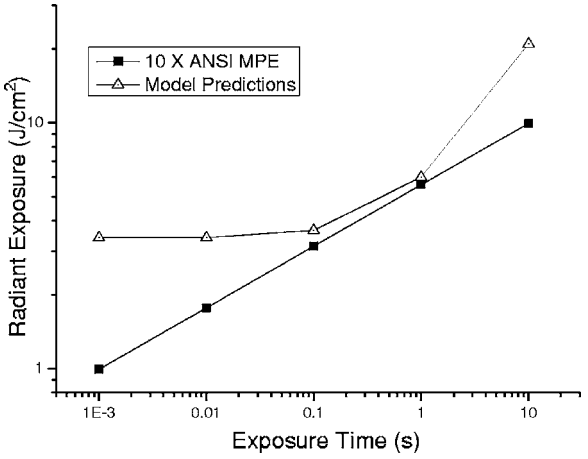

Fig. 10 The predicted damage threshold radiant exposures to 10.6 μm (CO_2 laser) and 2.0-μm laser irradiation and their corresponding ANSI MPE limits as a function of exposure duration. (Prediction of Gaussian shape irradiance, spot diameter=3.5 mm.)

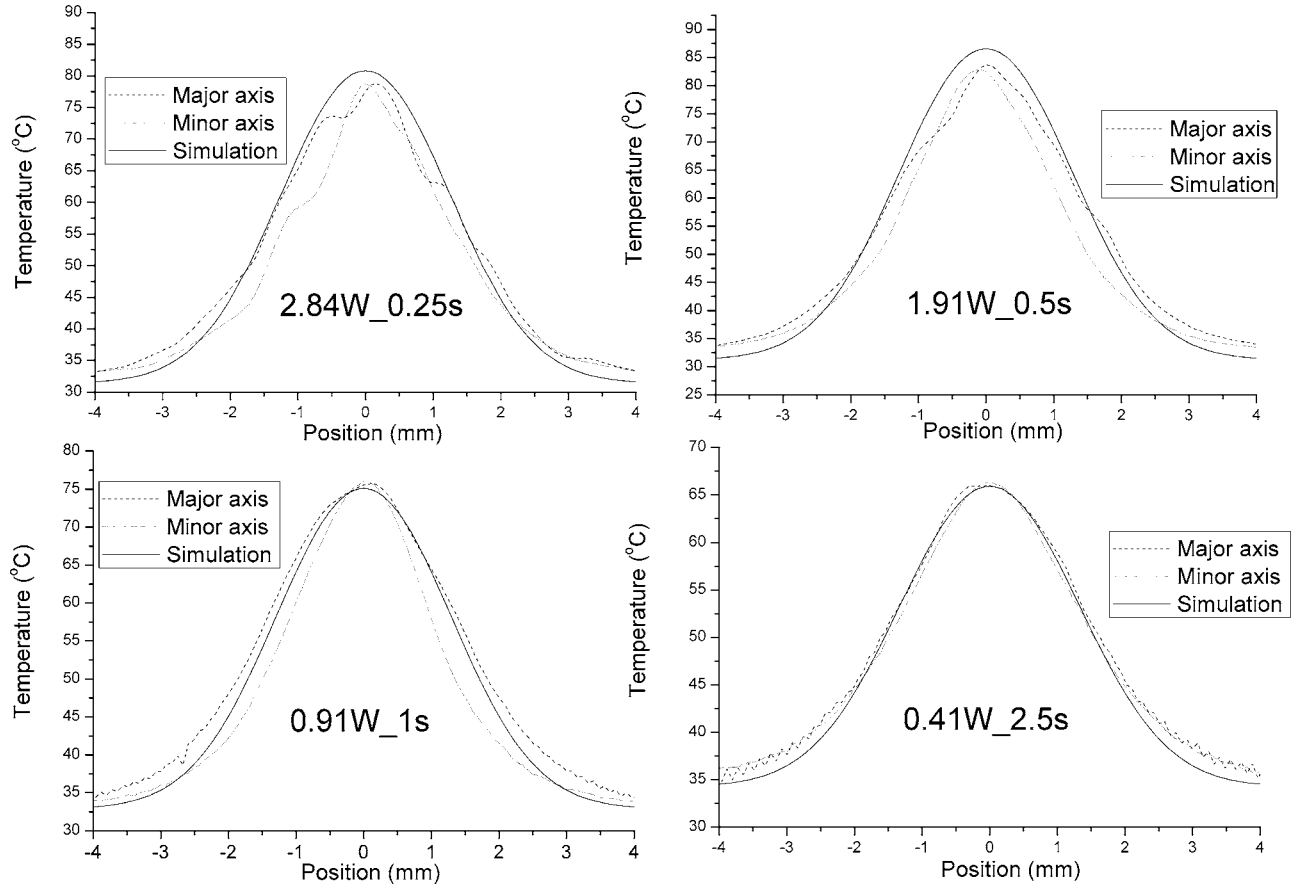

Fig. 11 The predicted radial temperature and experimental temperature distributions along major and minor axes after laser irradiation. Beam radius 2.44 mm.

10. For each exposure duration, however, there was little change in the associated threshold temperature. For our large spot sizes of irradiation, 4.88 to 13.84 mm diam, most of the heat was transferred along the axial direction rather than the radial direction.[19] Therefore, the shape of the temperature response curve depended less on the surface irradiance profile than axial light distribution, which was governed by Beer's law of absorption. This trend is not true for small spot sizes relative to optical penetration where radial heat conduction becomes significant.

The other end point of the damage threshold was defined as instant redness, that is, redness within 1 min of observation. Radiant exposures at the instant redness thresholds are compared with radiant exposures at the persistent redness thresholds in Table 2. The standard rate process model was used to compute Ω for the instant redness thresholds. The maximum Ω values at the center of the laser beam simulated by the model are presented in Table 5. When the exponential dependence of the damage integral on temperature [Eq. (9)] is considered, the values of Ω in Table 5 are not unreasonable. The point marked with a ☆ represents a large threshold for instant damage that exceeded the threshold for persistent damage. Nevertheless, the analysis for instant damage did not predict a finite damage radius. The standard rate process model described the irreversible damage process associated with the thermal denaturation of cells in the tissue. Furthermore, two parameters A and E_0 were obtained from experiments that studied the persistent damage to skin. The primary mechanism of instant redness to the skin was the increase of blood flow in the dermis, which was a reversible process without any cell denaturation. In conclusion, the standard rate process was not a good model for estimating the instant redness lesion on the skin, because the damage mechanisms for instant and persistent redness were different.

The ANSI Z136.1-2000 gives MPE limits for far-IR wavelengths between 1.8 and 2.6 μm as a function of laser exposure duration for a spot diameter of 3.5 mm and exposure durations between 10^{-3} and 10 s. Experimental results[3] revealed that the ANSI MPE standard was reasonable for the original 3.5-mm spot diameter and exposure durations from 0.25 to 2.5 s. Our model, however, was used to evaluate the ANSI MPE standard for a broader range of exposure durations. Table 6 shows the predicted radii and depths of thermal lesions ($\Omega=1$) with estimated threshold radiant exposures (ten times the ANSI MPE value $H_{\max}=0.56\ t^{0.25}$) and a 3.5-mm laser spot diameter. For exposure durations from 1 to 10^{-2} s, thermal lesions were less than 1 mm in radius, which was comparable to the values for the experimental sizes of skin thermal lesions at threshold (listed in Table 3). Most computed lesion depths at ten times the standard were less than the predicted depths at the measured persistent red-

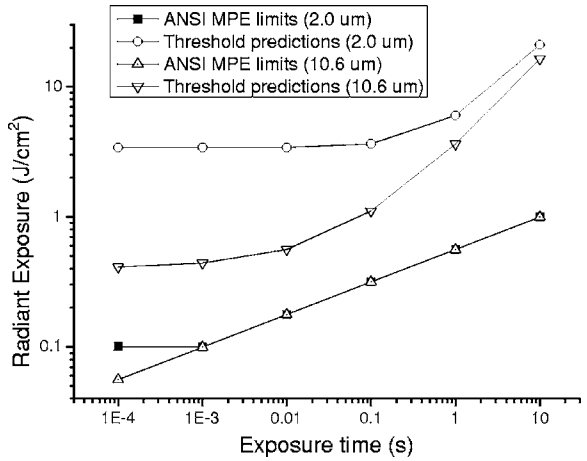

Fig. 12 The simulated threshold radiant exposure values compared with 10×ANSI MPEs as a function of laser exposure time. (Spot diameter=3.5 mm.)

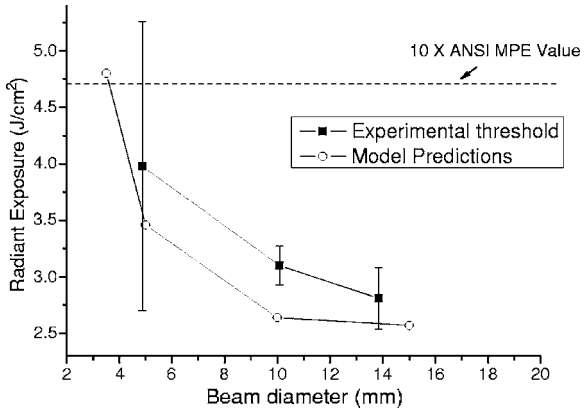

Fig. 13 The simulated threshold radiant exposure values (damage radius=1.0 mm) and experimental values (threshold average radiant exposure) compared to 10×ANSI MPE as a function of spot size. (Exposure duration=0.5 s.)

ness thresholds (listed in Table 4). Computed maximum Ω s were less than 1 for 10- and 10^{-3}-s exposure durations, indicating that no thermal damage occurred with the estimated threshold radiant exposures at those exposure conditions.

It should be noted that the value of the safety factor was based on considerations of the overall level of uncertainty in the data, the experimental detail, the sources of potential error, the differences between animal and humans, and the state of knowledge of the injury mechanism and the biological sequelae. Although a safety factor of less than ten has been used at times when experimental uncertainty was small, the value of ten for the safety factor has been adequate and is most frequently considered.[29] Therefore, the safety factor was chosen to be ten in this work.

Furthermore, we used the model to obtain a rough estimate of the MPE values. Based on the discussion before and the simulated and measured radii of the persistent redness lesions at threshold (see in Table 3), we assumed the following: 1. the second-degree burn threshold occurred when the radius of the surface lesion ($\Omega=1$) was equal to 1.0 mm, and 2. the estimation of MPE value was a factor of 10, which is called the safety factor below the radiant exposure at the second-degree burn threshold. The 1.0-mm damage radius was selected as a typical value from the range of experimental values given in Table 3. In Fig. 12, the simulated threshold radiant exposure values were compared with 10×ANSI MPE limits as a function of time for a laser spot of 3.5 mm diam. The comparison showed that the ANSI MPE values were close to or less than the corresponding estimations of MPE produced by the model.

In conclusion, as shown by the data in Table 6 and Fig. 12, the current ANSI MPE standard matches the model predictions for exposure durations from 10^{-1} to 1 s; however, the differences for exposure duration less than 0.1 s or longer than 10 s need to be examined. For exposure durations less than 0.1 s, the model predicts a nearly constant MPE. Generally, the damage that occurs at a point in the tissue is not only a function of the temperature increase, but it also depends on the rise time and decay characteristics of temperature. The characteristic thermal diffusion time in the skin is about 300 ms for 2000-nm laser irradiation and a large spot diameter. Therefore, for exposure durations less than 0.1 s, heat conduction during laser irradiation is negligible, and the threshold damage according to the damage integral is a function only of peak temperature at a point and its decay transient at the end of the short exposure.[30] In other words, the threshold radiant exposure, which is directly proportional to the temperature increase, is not a function of exposure duration in this range. Consequently, Fig. 12 shows that the ANSI MPE limits may be underestimations for laser pulses less than 0.1 s. Furthermore, Fig. 12 predicts a constant radiant exposure level for times between 0.001 to 0.1 s, and potentially for even shorter times. Currently, the ANSI MPE value is constant for exposure durations from 10^{-3} to 10^{-9} s. Our modeling results indicate that the range of a constant MPE could be extended to 10^{-1} s. The ANSI plateau level for exposure durations less than 0.001 s is 0.1 J/cm^2, whereas the model predicts a plateau level of about 0.34 J/cm^2 starting at 0.1 s. Although it has been suggested that the ANSI MPE level may be too low for exposure durations less than 0.1 s, caution should be exercised until further pigskin experimental data are available for this exposure duration range. For exposure time larger than 4 s (see Fig. 6), the model may underestimate temperatures due to its overestimation of evaporative cooling rate. Thus the temperature rise from a 10-s laser irradiation may be lower than the actual temperature and overestimate the MPE values.

The spot-size-dependent threshold radiant exposure values were simulated by the model, and in Fig. 13 they are compared with the experimental results. The experimental study of the *in-vivo* pigskin damage threshold for beam diameters larger than 3.5 mm and exposure durations of 0.25 s and longer revealed that it may be necessary to revise the ANSI MPE standard to a lower value.[3] Both experimental values (threshold average radiant exposure) and the model simulation for a lesion radius of 1.0 mm imply that the predicted MPE values are less than the ANSI standard for the large beam diameters. Our data support the position that the MPE should be decreased as the beam diameter becomes larger than 3.5 mm. In summary, both experiment and simulation support the need to revise the MPE standard for far-IR laser

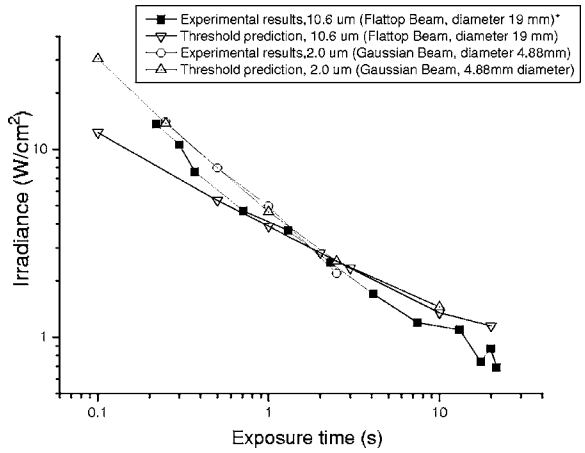

Fig. 14 The experimental threshold irradiance levels for both 2.0- and 10.6-μm wavelengths laser irradiation and their corresponding model predictions. * refers to Ref. 30.

beams with large diameters (>3.5 mm). Clearly, the model provides a system for studying the relationships between MPE value and spot size, exposure duration, and wavelength.

In Fig. 9, the simulated damage threshold radiant exposures for CO_2 (10.6 μm) laser irradiation are compared with the published pigskin damage threshold data.[27] The higher prediction of threshold radiant exposure at 20 s was due to the overestimation of evaporative cooling rate. Excluding that point, good agreement was observed between the optical-thermal-damage model and experimental results. By adjustment of optical parameters as a function of wavelength, predictions are possible as a function of exposure duration and spot size at exposure duration less than 10 s and at laser wavelengths where water is the primary absorber and scattering is insignificant.

The predicted damage thresholds to 10.6 μm (CO_2 laser) and 2.0-μm laser irradiation as a function of exposure duration are compared in Fig. 10. For 10.6-μm wavelength irradiation, Fig. 10 predicts a constant radiant exposure level for time between 0.0001 to 0.001 s, assuming linear heat conduction. Because the characteristic thermal diffusion time in the skin for 10.6-μm wavelength irradiation is approximately 100 times less than that for 2.0-μm wavelength,[30] the time range of constant radiant exposure level for 10.6-μm wavelength ends at 0.001 s instead of 0.1 s for 2.0-μm wavelength. At 10.6-μm wavelength, the safety factors of the predicted threshold radiant exposure with respect to ANSI MPE level are less than 10 at exposure time from 10^{-4} to 3 s. Further damage experiments may be necessary to examine the suitability of the ANSI MPE limits for the 10.6-μm wavelength.

Figure 14 shows the experimental threshold irradiance for both 2.0- and 10.6-μm wavelengths laser irradiation and their corresponding model predictions of threshold irradiance. Both experimental and simulated data indicate that a simple power law could be used to describe the relation between threshold irradiance and exposure time:

$$E = At^{-B}, \tag{15}$$

where E is the threshold irradiance, t is the exposure time, and A and B are two constant coefficients. The irradiance-time power law has been discussed in our previous work.[3]

We were aware of the limitations of our model in that several physical processes were excluded from the model analysis. For instance, the model used for the 2000-nm wavelength did not incorporate photon scattering in skin, nor did it address changes in the optical and thermal properties of the tissue due to the temperature increase. Furthermore, the temperature gradients in skin induced water transport in the tissue from deeper layers to the surface, which may in turn have had a significant effect on the heat and mass transfer and light absorption coefficients; in other words, the heat deposition rate and surface evaporation kinetics may need more consideration in respect to the temperature change. Another important source of uncertainty will always be human judgment in estimating lesion radii for large spot sizes (see Table 3).

Perhaps new technology will provide a method for replacing our qualitative visualization of damage with a more quantitative way. For example, polarization-sensitive optical coherence tomography measurements may provide an *in-vivo* method for measuring birefringence loss owing to thermal denaturation in tissue. Moreover, if it is possible to quantitatively and separately record thermal damage of each constituent in tissue, a multiple damage process model that includes several standard Arrhenius integrals could be developed. Each integral would predict damage of one specific constituent in tissue.

5 Conclusion

An optical-thermal-damage model precisely predicts the temperature and thermal damage in pigskin for 2000-nm laser irradiation. The information provided by the model allows us to 1. predict temperatures and the occurrence and size of thermal lesions in the skin, 2. evaluate the applicability of the standard rate process model for different thermal lesion endpoint definitions, 3. provide trends and identify experimental data that do not follow experimental trends, and 4. predict and test the ANSI MPE laser safety standard for a 2000-nm wavelength, exposure durations between 10^{-3} to 10 s, and various spot sizes.

The model verifies the suitability of the ANSI MPE standard for a wavelength of 2000 nm with a 3.5-mm spot size and exposure durations from 0.1 to 1 s. Compared to the published ANSI MPE standard, however, the model predictions give higher MPE values for exposure durations less than 0.1 s. The model suggests that the ANSI MPE exposure duration range for short pulses should be extended to a larger range of 10^{-1} to 10^{-9} s at a constant or plateau level of radiant exposure.

According to the model predictions, when the laser beam diameter is larger than 3.5 mm, it may be necessary to lower the values of the ANSI MPE standard if a safety factor of ten is used to derive MPE values. This conclusion is consistent with the *in-vivo* pigskin experimental results.[3]

In conclusion, the optical-thermal-damage model, supported by experimental validation, provides a system for predicting the thermal response of skin to laser irradiation and

the damage caused by such irradiation. By adjustment of the optical parameters as a function of wavelength, predictions are possible as functions of exposure duration and spot size at the laser wavelength where water is the primary absorber and scattering is insignificant.

Acknowledgments

Opinions, interpretations, conclusions, and recommendations are those of the authors and are not necessarily endorsed by the University of Texas at Austin, the United States Air Force, or the U.S. Department of Defense. The authors wish to thank Karl Schulmeister, Junghwan Oh, and Daniel C. O'Dell for their kind help. Contract grant sponsors are Northrop Grumman Information Technology, The Albert and Clemmie Caster Foundation.

References

1. American National Standards Institute, *ANSI Z136.1-2000, American National Standard for Safe Use of Lasers*, Laser Institute of America, Orlando, FL (2000).
2. J. A. Zuclich, D. J. Lund, B. E. Stuck, and P. R. Edsall, "Wavelength dependence of ocular thresholds in the near-IR to far-IR transition region (proposed revisions to MPEs)," *Proc. 2005 Intl. Laser Safety Conf.*, Marina del Rey, CA, Jan. 2005, Laser Institute of America.
3. B. Chen, D. C. O'Dell, S. L. Thomsen, B. A. Rockwell, and A. J. Welch, "Porcine skin ED50 damage thresholds for 2000 nm laser irradiation," *Lasers Surg. Med.* (to be published).
4. T. A. Eggleston, W. P. Roach, M. A. Mitchell, K. Smith, D. Oler, and T. E. Johnson, "Comparison of two porcine (Sus scrofa domestica) skin models for in vivo near-infrared laser exposure," *Comp. Med.* **50**(4), 391–397 (2000).
5. M. H. Niemz, *Laser-Tissue Interactions*, Springer-Verlag, Berlin (1996).
6. M. A. Mainster, T. J. White, and R. G. Allen, "Spectral dependence of retinal damage produced by intense light sources," *J. Opt. Soc. Am.* **60**(6), 848–855 (1970).
7. M. A. Mainster, T. J. White, J. H. Tips, and P. W. Wilson, "Transient thermal behavior in biological systems," *Bull. Math. Biophys.* **32**, 303–314 (1970).
8. A. Vassiliadis, H. C. Christian, and K. G. Dedrick, "Ocular laser threshold investigations," USAF School of Aerospace Medicine, Standford Research Institute, Brooks Air Force Base, TX (1971).
9. A. J. Welch, "Model of thermal injury based on temperature rise in fundus exposed to laser radiation," USAF School of Aerospace Medicine, Brooks Air Force Base, TX (1975).
10. A. N. Takata, "Thermal model of laser-induced eye damage," Engineering Mechanics Division, IIT Research Institute, 10 West 35th, Chicago, IL (1974).
11. A. N. Takata, "Laser-induced thermal damage of skin," USAF School of Aerospace Medicine, Brooks Air Force Base, TX (1977).
12. C. P. Cain and A. J. Welch, "Measured and predicted laser-induced temperature rises in the rabbit fundus," *Invest. Ophthalmol.* **13**(1), 60–70 (1974).
13. E. H. Wissler, "An analysis of chorioretinal thermal response to intense light exposure," *IEEE Trans. Biomed. Eng.* **23**(3), 207–215 (1976).
14. J. A. Scott, "The computation of temperature rises in the human eye induced by infra-red radiation," *Phys. Med. Biol.* **33**, 243–257 (1988).
15. E. H. Wissler, "An analytical solution countercurrent heat transfer between parallel vessels with a linear axial temperature gradient," *J. Biomech. Eng.* **110**(3), 254–256 (1988).
16. R. Birngruber, F. Hillenkamp, and V. P. Gabel, "Theoretical investigations of laser thermal retinal injury," *Health Phys.* **48**(6), 781–796 (1985).
17. G. Yoon, A. J. Welch, M. Motamedi, and M. J. C. van Gemert, "Development and application of three-dimensional light distribution model for laser irradiated tissue," *IEEE J. Quantum Electron.* **QE-23**(19), 1721–1733 (1987).
18. J. H. Torres and M. Motamedi, "Experimental evaluation of mathematical-models for predicting the thermal response of tissue to laser irradiation," *Appl. Opt.* **32**(4), 597–606 (1993).
19. S. L. Jacques, "Role of tissue optics and pulse duration on tissue effects during high-power laser irradiation," *Appl. Opt.* **32**(13), 2447–2454 (1993).
20. L. O. Svaasand, T. Boerslid, and M. Oeveraasen, "Thermal and optical properties of living tissue: application to laser-induced hyperthermias," *Lasers Surg. Med.* **5**(6), 589–602 (1985).
21. F. P. Incropera and D. P. Dewitt, *Fundamentals of Heat and Mass Transfer*, 5th ed., John Wiley and Sons, New York (2001).
22. S. H. Diaz-Valdes, G. Aguilar, R. Basu, E. J. Lavernia, and B. J. Wong, "Modeling the thermal response of porcine cartilage to laser irradiation," in *Laser-Tissue Interaction XIII: Photochemical, Photothermal, and Photomechanical*, pp. 47–56 (2002).
23. A. R. Moritz and F. C. Henriques, Jr., "Studies of thermal injury: II. The relative importance of time and surface temperature in the causation of cutaneous burns," *Am. J. Pathol.* **23**, 695–720 (1947).
24. F. F. Henriques, "Studies of thermal injury V: The predictability and the significance of thermally induced rate processes leading to irreversible epidermal injury," *Arch. Pathol.* **43**, 489–502 (1947).
25. D. J. Finney, *Probit Analysis*, 3rd ed., Cambridge University Press, New York (1971).
26. G. M. Hale and M. R. Querry, "Optical constants of water in the 200 nm to 200 μm wavelength region," *Appl. Opt.* **12**, 555–563 (1973).
27. A. S. Brownell, W. H. Parr, and D. K. Hysell, "Skin and carbon dioxide laser radiation," *Arch. Environ. Health* **18**, 437–442 (1969).
28. J. A. Pearce, S. Thomsen, H. Vijverberg, and T. McMurray, "Kinetics for birefringence changes in thermally coagulated rat skin collagen," *Proc. SPIE* **1876**, 180–186 (1993).
29. D. H. Sliney, J. Mellerio, V. P. Gabel, and K. Schulmeister, "What is the meaning of threshold in laser damage experiments? Implications for human exposure limits," *Health Phys.* **82**, 35–347 (2002).
30. L. A. Priebe and A. J. Welch, "Asymptotic rate process calculations of thermal injury to the retina following laser irradiation," *J. Biomech. Eng.* **100**, 49–54 (1978).